Journal of Environmental Protection, 2020, 11, 807-820
https://www.scirp.org/journal/jep
ISSN Online: 2152-2219
ISSN Print: 2152-2197

X-Ray Absorption Spectroscopy Analysis of Lead Species Adsorbed on Various Oxides from High pH Solution

Takanori Miyake[1], Tetsuo Honma[2], Hiroshi Arimatsu[1], Hiroto Fukunishi[1], Huimin Liu[1], Makoto Sano[1], Yuuki Kakutani[1], Mitsumasa Okada[1], Kaori Shimizu[1], Setsuo Yoshida[3], Kazumasa Suetsugu[3]

[1]Faculty of Urban and Environmental Engineering, Kansai University, Suita, Osaka, Japan
[2]Japan Synchrotron Radiation Institute (JASRI), Sayo-cho, Hyogo, Japan
[3]TOSOH Corporation, Shunan, Yamaguchi, Japan
Email: tmiyake@kansai-u.ac.jp

How to cite this paper: Miyake, T., Honma, T., Arimatsu, H., Fukunishi, H., Liu, H., Sano, M., Kakutani, Y., Okada, M., Shimizu, K., Yoshida, S. and Suetsugu, K. (2020) X-Ray Absorption Spectroscopy Analysis of Lead Species Adsorbed on Various Oxides from High pH Solution. *Journal of Environmental Protection*, **11**, 807-820.
https://doi.org/10.4236/jep.2020.1110050

Received: August 27, 2020
Accepted: October 9, 2020
Published: October 12, 2020

Abstract

Lead dissolved in water must be removed in order not to cause diseases, especially from high pH aqueous solution. Various oxides having high specific surface area are often applied to remove lead in water media. To improve removal ability for lead species, it is necessary to understand the adsorbed structure of lead species on oxides. At first, the adsorption behavior of lead from high pH solution in the presence of Ca^{2+} and Na^{+} was compared. Lead and calcium species were adsorbed up to the monolayer, and the adsorption isotherm was analyzed as Langmuir-type adsorption. In the presence of Ca^{2+}, the amount of removed lead was reduced. To clarify this influence of Ca^{2+}, X-ray absorption spectroscopy was adopted. It was for the first time revealed that lead species at pH > 12 and pH < 10.5 differed, and that lead species adsorbed on various oxides had a similar structure.

Keywords

X-Ray Absorption Spectroscopy, Water Purification, Lead Removal, Manganese Oxide, Adsorption

1. Introduction

In our daily life, a large amount of wastes such as domestic garbage, used plastics, and papers, are disposed. These wastes, called municipal wastes, are incinerated, which leave ash to be withdrawn from the bottom of the incinerator and fly ash to be collected by the electric dust collector. The fly ash contains signifi-

cant amounts of poisonous elements such as lead and cadmium, and causes problems when buried [1] [2] [3] [4]. This is because calcium hydroxide solution is sprayed onto the fly ash to neutralize hydrogen chloride and sulfur oxides. Then, when the fly ash is buried and rain reaches the buried ash, the pH of the eluent can reach as high as pH 12, which leads to dissolution of lead. To prevent dissolution of lead, the fly ash is solidified into cement or is chemically treated using chelate compounds [5]. The former method necessitates a special facility and is costly. In the latter method, chelate compounds are expensive and gradually degrade after months, releasing lead. Thus, a better and preferably permanent treatment for lead from the fly ash is needed.

There have been many reports to make heavy metals immobilize with SiO_2 and Al_2O_3 [6] [7] [8] [9] [10]. Studies on adsorption using mesoporous materials have also been reported [11]-[22]. However, these methods cannot be adopted for lead removal because SiO_2, Al_2O_3, and most of the mesoporous materials dissolve into high pH aqueous solution. Mesoporous manganese oxide having a large surface area has been reported [23] [24] [25]. Papers dealing with lead removal using manganese oxide are reported; however, no papers adopted pH higher than neutral to the best of our knowledge. Manganese oxides do not dissolve under high pH conditions caused by the sprayed calcium hydroxide and are not expensive.

In this paper, at first we studied lead removal from a high pH 12.4 aqueous solution using mesoporous manganese oxide as an adsorbent. Then, the lead species adsorbed under high pH of 12.4 on various oxides was analyzed especially with X-ray absorption spectroscopy.

2. Experimental

2.1. Preparation of Mesoporous Manganese Oxide

Into 50 mL of distilled water, 10 mmol of potassium permanganate was dissolved. Then, 3.3 mmol of maleic acid in 50 mL of distilled water was added as a reducing agent and the mixture was stirred for 1 h. After aging for 24 h at room temperature, the resulting black precipitate was washed with distilled water. After drying at 70˚C overnight, the mesoporous manganese oxide (Meso-Mn) was obtained by calcination in air at 300˚C for 2 h.

For comparison, SiO_2 (Q-10; Fuji Silysia Chemical Ltd., Japan), Al_2O_3 (KHD-24; Sumitomo Chemical Co. Ltd., Japan), and ZrO_2 (JRC-ZRO-5; Catalysis Society of Japan) were also used to remove lead.

2.2. Removal of Lead from pH 12.4 Aqueous Solution

2.2.1. Preparation of Lead Solution of pH 12.4

Into 1000 mL of distilled water, 2.02 g (27.3 mmol) of $Ca(OH)_2$ was added. The container was sealed so that no CO_2 dissolved into the alkaline solution. The content was agitated for 1 h in order to saturate $Ca(OH)_2$ and stood still at room temperature for 3 d. By filtration, a solution saturated with $Ca(OH)_2$ was ob-

tained. The pH of this solution was measured with a pH meter to be 12.4. Into this solution, 0.16 - 1.28 g (0.48 - 3.84 mmol) of $Pb(NO_3)_2$ was dissolved. Thus, a solution containing a desired concentration of lead at pH 12.4 was prepared.

2.2.2. Removal of Lead

Typically, into 100 mL of the prepared lead solution, a 0.20 g portion of Meso-Mn was added, and the mixture was stirred with a Teflon-coated stirrer bar for 1 min to 240 h at room temperature. The removal was carried out in a sealed glass Erlenmeyer flask, preventing dissolution of CO_2 into the alkaline solution. After adsorption of lead, Meso-Mn was centrifuged and the concentrations of lead and calcium species in the supernatant were analyzed with Inductively Coupled Plasma (ICP) spectroscopy (ICPS-7510, Shimadzu Corp., Japan). When the influence of co-existing calcium was investigated, NaOH was used instead of $Ca(OH)_2$ to control pH.

2.3. Characterization

The powder X-ray diffraction (XRD) patterns were obtained with RMT-18kWHFVE (Rigaku, Japan) with Cu Kα-radiation at 40 kV and 20 mA. N_2 adsorption-desorption isotherms were obtained with BELSORP-mini2 (MicrotracBEL, Japan), and the pore size distribution (BJH method) and BET surface area were calculated based on the adsorption-desorption isotherms. The elemental analysis was carried out using ICP. The analysis sample was prepared by dissolving 0.050 g of a solid before or after removal of lead in 20 mL of 10 $mol \cdot L^{-1}$ HNO_3 with a few drops of 30 wt% H_2O_2 aqueous solution. Before measurement, the solution was diluted to a desired concentration range.

The zeta potential was measured by the laser Doppler method with Zetasizer Nano-Z (ZEN2600, Malvern Instruments Inc., United Kingdom). For the measurement, 0.020 g of powder sample was dispersed in distilled water. The pH of the suspension was arranged with aqueous HCl, NaOH or $Ca(OH)_2$ solution. X-ray photoelectron spectra (XPS) were recorded by JEOL JPS-9000MX (JEOL, JAPAN) with Mg Kα-radiation at 10 kV and 10 mA, and the peak position was calibrated with $Pt_{4f7/2}$ at 70.9 eV as an internal standard.

X-ray absorption fine structure (XAFS) and X-ray absorption near edge spectrum (XANES) were obtained at 14B2 beamline at SPring-8, Japan. Silicon (311) crystal was used as a monochromator. For the measurement of Pb L_{III} edge of high Pb concentration samples, the transmission mode was adopted. For the low concentration samples, Pb L_{III} edge spectra were collected by the fluorescence mode using 19-element Ge semi-conductivity detector. Radial structure function was Fourier transformed for the XAFS vibration between wave number k of 2 and 8 $Å^{-1}$. Powder samples were pelletized together with boron nitride and solution samples were packed in polyethylene bag.

3. Results and Discussion

The preparation and characterization of mesoporous manganese oxide (Me-

so-Mn) have been reported elsewhere [24] [26]. In brief, Meso-Mn was amorphous (XRD) and mesoporous (inter-particle mesopores of about 5 nm) and had a high BET surface area of approximately 250 $m^2 \cdot g^{-1}$.

3.1. Removal of Lead at pH 12.4

The adsorption isotherm was studied in order to understand the mechanism of adsorption and the maximum amount of adsorption. When lead adsorption was carried out at pH 12.4 controlled with NaOH, a Langmuir-type adsorption phenomenon was observed (**Figure 1**) with a monolayer adsorption capacity of lead of 4.01 $mmol \cdot g^{-1}$. At pH 12.4, the concentration of co-existing Na^+ was varied by adding $NaNO_3$, and the influence of the concentration of Na^+ is indicated in **Figure 2**. From these results, it can be said that the existence of Na^+ does not influence the adsorption of lead.

Figure 3 shows the adsorption isotherm for calcium. Calcium also indicated the Langmuir-type adsorption, and the monolayer adsorption capacity was calculated to be 2.97 $mmol \cdot g^{-1}$. Then, adsorption of lead in the presence of Ca^{2+} was investigated (**Figure 4**). The adsorption behavior of lead could be analyzed again by the Langmuir-type equation. The analysis showed a monolayer adsorption capacity of 1.83 $mmol \cdot g^{-1}$. In addition, lead and calcium seemed to compete for the same adsorption site because the total amount of adsorption was almost constant at ca. 3.2 $mmol \cdot g^{-1}$. At saturation, the molar ratio of lead to calcium was close to unity, suggesting the formation of a specific complex.

To confirm the superiority of Meso-Mn, the removal of lead with SiO_2, Al_2O_3 and ZrO_2 was investigated. To make the comparison simple, oxides having surface areas similar to that of Meso-Mn were used. As shown in **Figure 5**, Meso-Mn

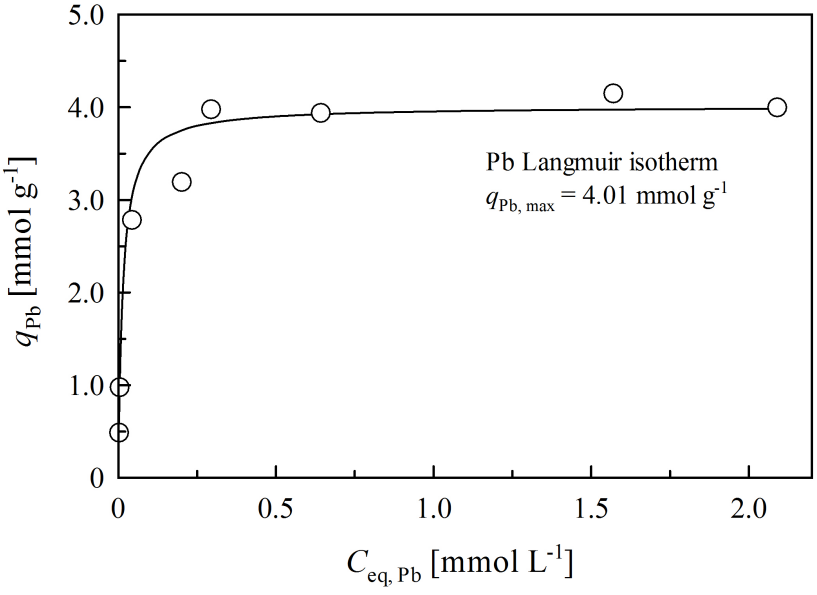

Figure 1. Adsorption isotherm of Pb with Meso-Mn under pH control with NaOH. Adsorbent: 0.050 g, Initial Pb concentration: 0 - 2.96 $mmol \cdot L^{-1}$, Initial Na concentration: 40.1 $mmol \cdot L^{-1}$, Solution: 100 mL, Initial pH: 12.4, Time: 240 h.

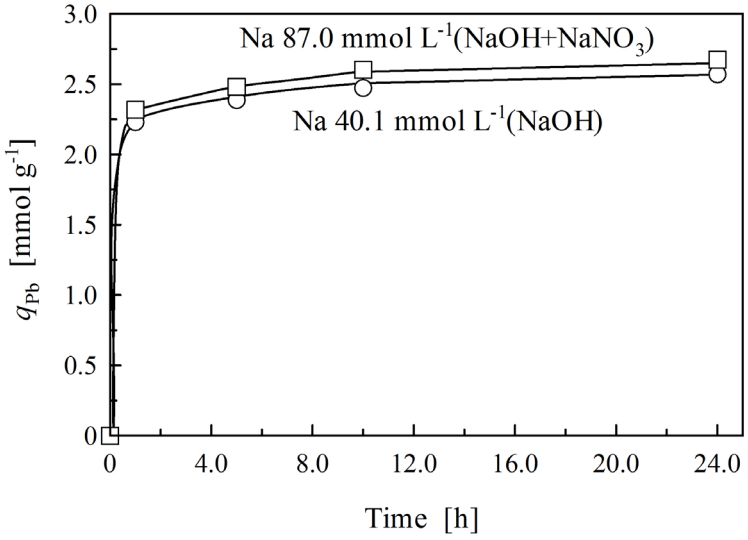

Figure 2. Influence of co-existence of Na on removal of Pb with Meso-Mn. Adsorbent: 0.050 g, Initial Pb concentration: 2.89 mmol·L^{-1}, Initial Na concentration: 40.1 mmol or 87.0 mmol·L^{-1}, Solution: 100 mL, Initial pH: 12.4, pH control: NaOH, Time: 0 - 24 h.

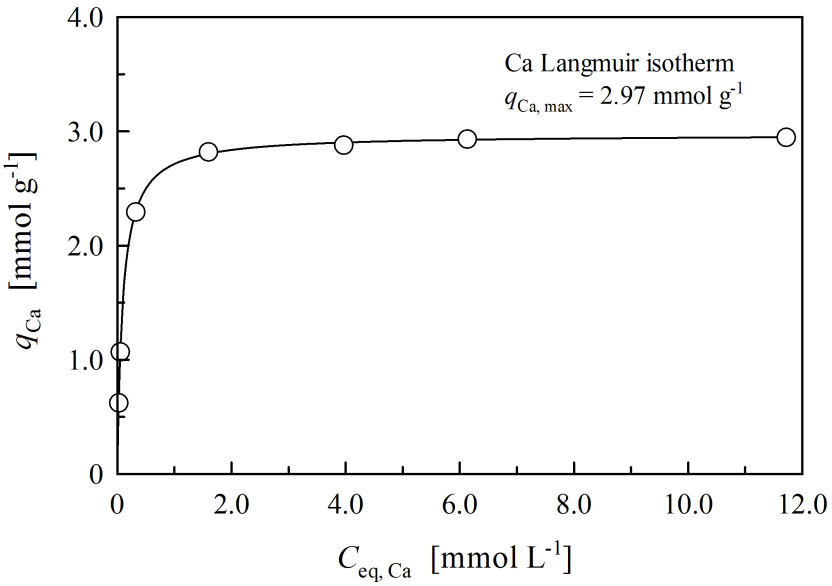

Figure 3. Adsorption isotherm of Ca with Meso-Mn. Adsorbent: 0.20 g, Initial Ca concentration: 0 - 19.2 mmol·L^{-1}, Solution: 100 mL, Initial pH: 12.4, pH control: NaOH, Time: 240 h.

and SiO_2 removed lead most. As SiO_2 also adsorbed a large amount of Ca^{2+}, Meso-Mn was the most selective for the lead removal. In addition, the dissolution of SiO_2 and Al_2O_3 themselves was confirmed for SiO_2 and Al_2O_3. Thus, Meso-Mn was the best choice for the removal of lead at a high pH of 12.

In summary for the adsorption of lead from the high pH solution, manganese oxide was the most promising adsorbent. The Langmuir-type adsorption was observed for both lead and calcium. Lead and calcium competed for the same adsorption site. It was suggested that lead and calcium formed a specific complex on Meso-Mn.

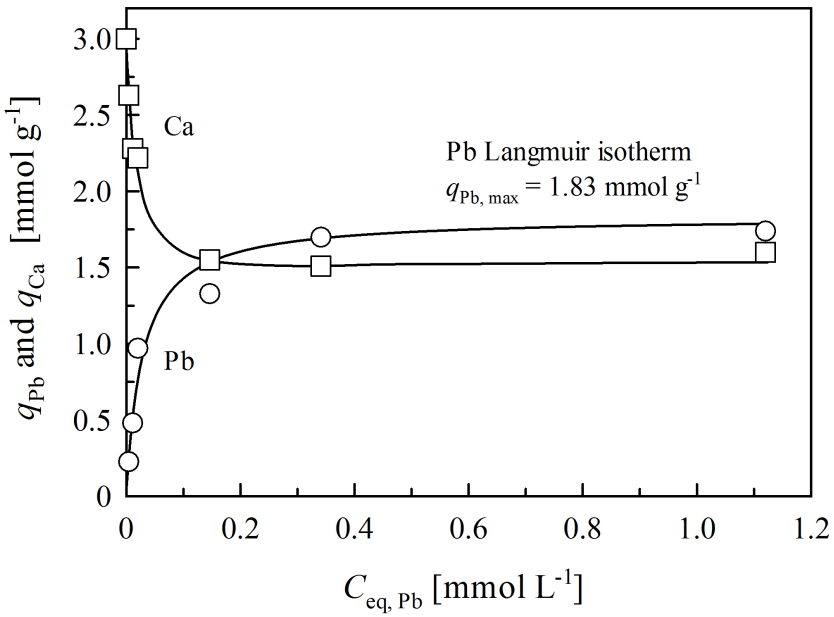

Figure 4. Adsorption isotherms of Pb and Ca with Meso-Mn. Adsorbent: 0.20 g, Initial Pb concentration: 0 - 3.86 mmol·L^{-1}, Initial Ca concentration: 19.2 mmol·L^{-1}, Solution: 100 mL, Initial pH: 12.4, pH control: $Ca(OH)_2$, Time: 240 h.

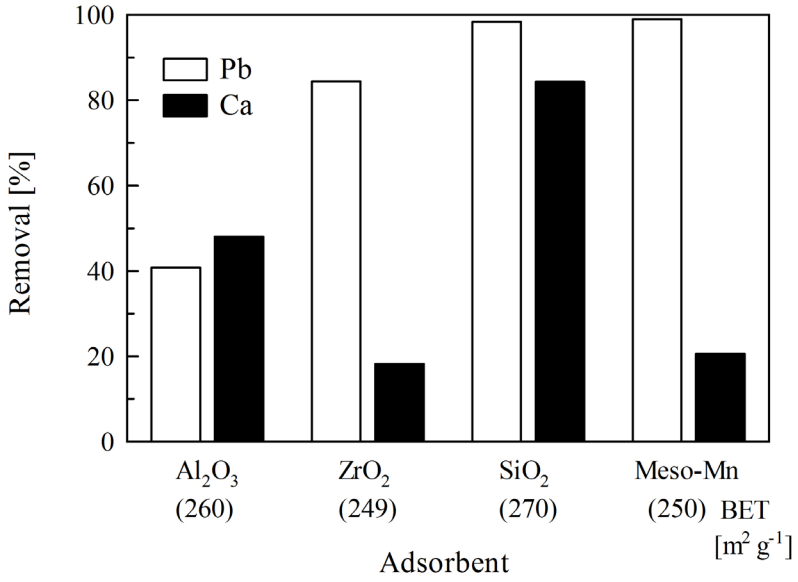

Figure 5. Removal of Pb and Ca with various metal oxides. Adsorbent: 0.20 g, Initial Pb concentration: 1.92 mmol·L^{-1}, Initial Ca concentration: 19.2 mmol·L^{-1}, Solution: 100 mL, Initial pH: 12.4, pH control: $Ca(OH)_2$, Time: 240 h.

3.2. X-Ray Absorption Spectroscopy

3.2.1. Lead Species in the Solution

The same XANES spectra, and therefore the same radial structure function, were observed for the lead species in solution between pH 4 and 10.5 (**Figure 6**). However, different XANES and XAFS spectra were observed at pH 12.4 (**Figure 7**). Up to pH 10.5, it is suggested from the coefficient of complex formation [27]

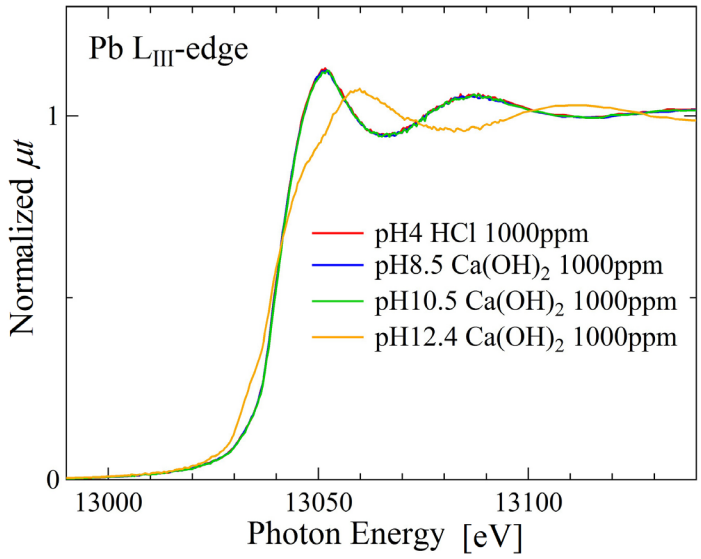

Figure 6. XANES spectra of lead species in the solution of various pH controlled with $Ca(OH)_2$. Pb concentration: 1000 ppm.

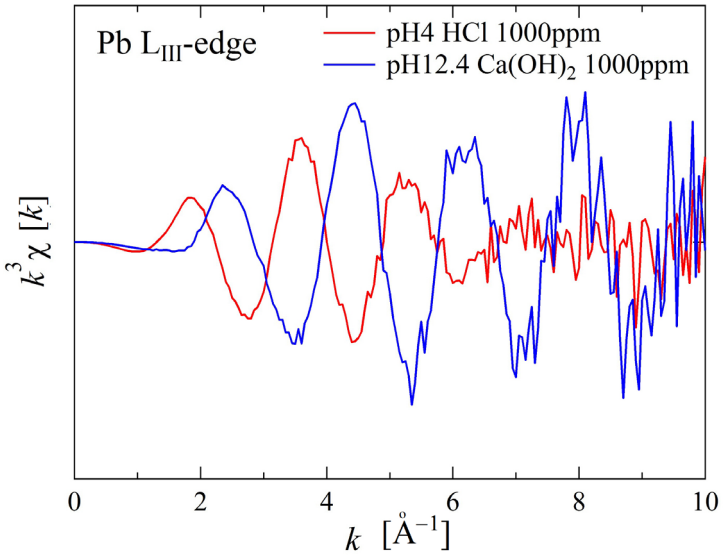

Figure 7. EXAFS vibration spectra for lead species in the solution at pH 4 and pH 12.4. Pb concentration: 1000 ppm.

that lead exists as Pb^{2+}, $Pb(OH)^+$ and $Pb(OH)_2$ (Electronic supplementary information **Figure S1**). On the other hand, $Pb(OH)_3^-$ is suggested at pH 12.4. Thus, it was revealed that when lead existed as cationic or neutral species, the structure of the first coordination sphere was the same. This is the first XANES information reported for lead in alkaline media.

For the XANES spectra at pH 12.4, different spectra were obtained when $Ca(OH)_2$ and NaOH were used as the pH controller (**Figure 8**). This may be because $Ca(OH)^+$ in the $Ca(OH)_2$ solution (Electronic supplementary information **Figure S2**) could have Coulomb interaction with $Pb(OH)_3^-$ while in NaOH solution this kind of interaction did not occur.

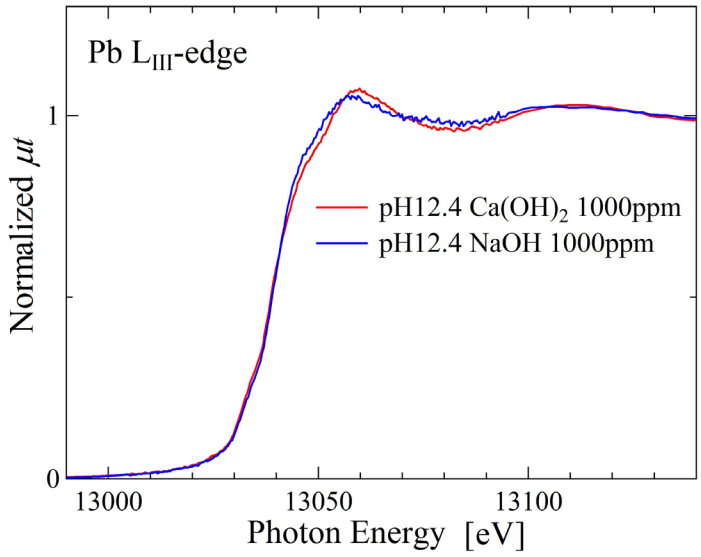

Figure 8. XANES spectra for lead species in the solution at pH 12.4 controlled with $Ca(OH)_2$ or NaOH. Pb concentration: 1000 ppm.

3.2.2. Lead Species Adsorbed on Oxides

When the concentration of lead was 3000 ppm in the presence of $Ca(OH)_2$, the highest concentration in the experiment, the solution was not transparent and a white suspension was observed. The distance from lead to the first coordination sphere oxygen in the suspension (**Figure 9**) coincided with those for lead species adsorbed on oxides, Meso-Mn (MnO_2), SiO_2, Al_2O_3 and ZrO_2 (**Figure 10**), suggesting that the same lead species was adsorbed on each oxide. Furthermore, the same XANES spectra were obtained for different amount of lead adsorbed on oxides, suggesting that the structure of adsorbed species does not depend on the amount of lead adsorbed on oxides.

As in **Figure 5**, depending on the adsorbents, the amounts of lead and calcium adsorbed on oxides were different, meaning different cation selectivity. On Meso-Mn and ZrO_2, the molar ratio of Pb to Ca was about unity. On the other hand, a few times more Ca than Pb adsorbed on Al_2O_3 and SiO_2. The dissolution of Al_2O_3 and SiO_2 surface was observed *vide supra* under highly alkaline solution of pH 12.4, and dissolved aluminic acid or silicic acid might have formed calcium aluminate or calcium silicate on Al_2O_3 and SiO_2, respectively. In the radial structure function for Al_2O_3 and SiO_2 (**Figure 10**), small peaks could be noticed in the second or third coordination sphere and this is different from the phenomenon for MnO_2 which does not dissolve in the highly alkaline conditions.

Thus, the behavior of lead in the highly alkaline conditions was analyzed for the first time and this information is very important to develop excellent materials to remove lead in water.

3.3. Adsorbed Species

First, the species of lead and calcium in the solution at different pH were estimated by the coefficient of complex formation [27] (Electronic supplementary

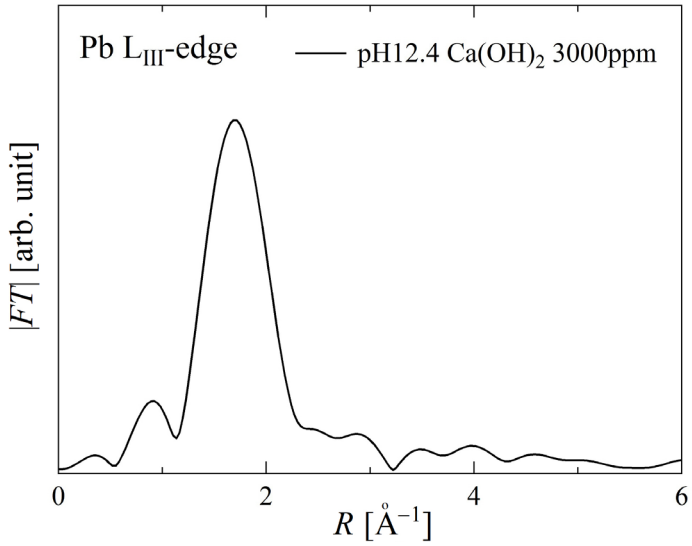

Figure 9. Radial structure function for high concentration lead suspension at pH 12.4 controlled with $Ca(OH)_2$. Pb concentration: 3000 ppm.

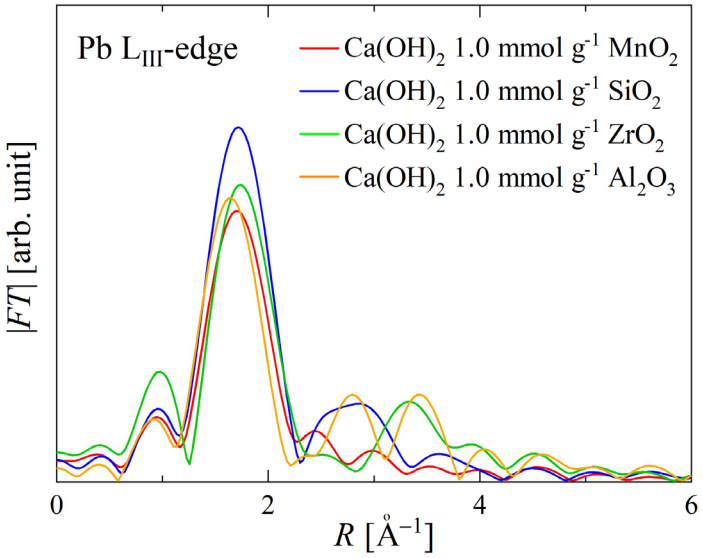

Figure 10. Radial structure function of lead species adsorbed on various oxides. Initial pH: 12.4, pH control: $Ca(OH)_2$, Pb: 1.0 mmol·g^{-1}.

information **Figure S1**, **Figure S2**). As mentioned in 3.2.1, lead exists as Pb^{2+}, $Pb(OH)^+$, $Pb(OH)_2$, and $Pb(OH)_3^-$, and the main lead species at pH 12.4 is estimated to be $Pb(OH)_3^-$. Similarly, calcium exists as Ca^{2+} and $Ca(OH)^+$, and both species may exist almost equally at pH 12.4. It is important that both anionic $Pb(OH)_3^-$ and cationic $Ca(OH)^+$ exist at pH 12.4.

The zeta potential of Meso-Mn at pH 12.4 was ca. −30 mV, when pH was controlled with NaOH. On the other hand, when the zeta potential was measured at pH 12.4 under pH control with $Ca(OH)_2$, the zeta potential was ca. +20 mV. Considering the fact that the co-existence of Na^+ had no influence on the adsorption of lead (*vide supra*), Na^+ did not adsorb on Meso-Mn. In contrast,

calcium species were adsorbed on Meso-Mn, and the charge on Meso-Mn became positive. Thus, the adsorption of lead species on Meso-Mn at pH 12.4 controlled with $Ca(OH)_2$ may be by an electrostatic interaction between negative species, $Pb(OH)_3^-$, and a positive surface bearing $Ca(OH)^+$. This is in accordance with the results by XANES in **Figure 8**.

To directly investigate the adsorbed lead species, Meso-Mn was dried at 80˚C overnight after the adsorption of lead, and analyzed with XRD. No distinct diffraction pattern related to lead species could be observed, even though the amount of lead was sufficiently high to be detected with XRD (data not shown). This may be because the lead species existed in the form of a monolayer. Even if lead existed as $Pb(OH)_2$, the stability of $Pb(OH)_2$ has been questioned [28], and observing the diffraction pattern of $Pb(OH)_2$ may be difficult.

The valence state of lead was studied with XPS of Pb $4f_{7/2}$ (**Figure 11**) and the valence of lead was 2+. XPS of the commercial reagent PbO showed its peak at 137.4 eV. From the binding energy, lead might have adsorbed as PbO. However, as mentioned above, it is known that $Pb(OH)_2$ is unstable [28], and therefore the possibility cannot be excluded that $Pb(OH)_2$ or $Pb(OH)_3^-$ changed to PbO during the drying process.

Some researchers reported the adsorption of hydrated Pb species or other divalent cations such as Ni^{2+} and Ca^{2+} on a variety of adsorbents using EXAFS [29] [30] [31]. Under neutral conditions, adsorption of hydrated Pb^{2+} is estimated [29] [30]. Bargar *et al.* reported that hydrated lead lost some of hydrated water on adsorption [29]. As far as we know, there are no reports by EXAFS on the adsorbed lead species under high pH conditions.

As discussed above, we do not have any decisive idea for the adsorbed lead species at this moment. However, considering the equimolar adsorption of lead and calcium, the existence of Pb-O bond and the valence of lead to be 2+, we

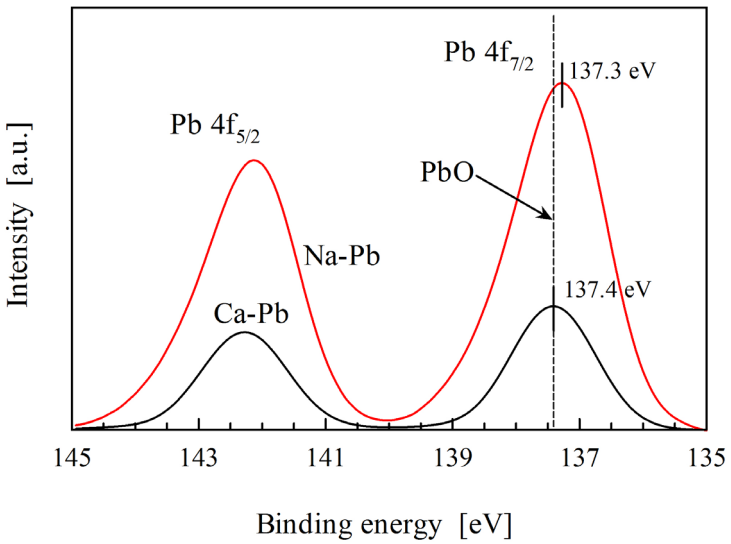

Figure 11. XPS spectra for Pb 4f adsorbed on Meso-Mn. pH control: $Ca(OH)_2$ for Ca-Pb and NaOH for Na-Pb.

may hypothesize the existence of a double hydroxide composed of lead and calcium of a probable formula of $CaPb(OH)_4$.

4. Conclusions

Lead adsorption on oxides from a high pH aqueous solution was studied and manganese oxide was the most promising adsorbent. It was suggested that lead and calcium species competed for the same adsorption site on manganese oxide and the amount of removed lead reached 1.8 $mmol \cdot g^{-1}$ under the co-existence of calcium hydroxide. The structure of lead species in the solution was different at pH 12.4 and at pH lower than 10.5. The adsorbed lead species was not made clear; however, a double hydroxide composed of lead and calcium like $CaPb(OH)_4$ was estimated. This information is very important to develop materials to remove lead in high pH water from the buried waste.

Based on the knowledge obtained, more promising material would be prepared by a monolayer loading of manganese oxide on a support of higher surface area than about 300 $m^2 \cdot g^{-1}$.

Acknowledgements

Part of the research was financially supported by "Strategic Project to Support the Formation of Research Bases at Private Universities": Matching Fund Subsidy from Ministry of Education, Culture, Sports, Science and Technology, 2012-2016. The synchrotron radiation experiments were performed at BL14B2 in the SPring-8 with the approval of the Japan Synchrotron Radiation Research Institute (JASRI) (Proposal No. 2015B1634). Part of the research was also financially supported by the Kansai University Fund for Domestic and Overseas Research Fund, 2018 and by the Kansai University Fund for the Promotion and Enhancement of Education and Research, 2019.

Conflicts of Interest

The authors declare no conflicts of interest regarding the publication of this paper.

References

[1] Nowak, B., Pessl, A., Aschenbrenner, P., Szentannai, P., Mattenberger, H., Rechberger, H., Hermann, L. and Winter, F. (2010) Heavy Metal Removal from Municipal Solid Waste Fly Ash by Chlorination and Thermal Treatment. *Journal of Hazardous Materials*, **179**, 323-331. https://doi.org/10.1016/j.jhazmat.2010.03.008

[2] Wang, L., Jin, Y. and Nie, Y. (2010) Investigation of Accelerated and Natural Carbonation of MSWI Fly Ash with a High Content of Ca. *Journal of Hazardous Materials*, **174**, 334-343. https://doi.org/10.1016/j.jhazmat.2009.09.055

[3] Karin, K.F., Christian, E., Gunnar, S. and Britt-Marie, S. (2010) Removal of Hazardous Metals from MSW Fly Ash—An Evaluation of Ash Leaching Methods. *Journal of Hazardous Materials*, **173**, 310-317. https://doi.org/10.1016/j.jhazmat.2009.08.094

[4] Olli, D., Hannu, N., Risto, P. and Gary, W. (2009) Comparison of the Characteristics of Bottom Ash and Fly Ash from a Medium-Size (32 MW) Municipal District Heating Plant Incinerating Forest Residues and Peat in a Fluidized-Bed Boiler. *Fuel Processing Technology*, **90**, 871-878. https://doi.org/10.1016/j.fuproc.2009.04.013

[5] Kamikita, M. (2005) Haikibutsu Shori Houhou. JP2005-3683025.

[6] Pena, M., Meng, X., Korfiatis, G.P. and Jing, C. (2006) Adsorption Mechanism of Arsenic on Nanocrystalline Titanium Dioxide. *Environmental Science & Technology*, **40**, 1257-1262. https://doi.org/10.1021/es052040e

[7] Wijnja, H. and Schulthessy, C.P. (2000) Vibrational Spectroscopy Study of Selenate and Sulfate Adsorption Mechanisms on Fe and Al (Hydr)oxide Surfaces. *Journal of Colloid and Interface Science*, **229**, 286-297. https://doi.org/10.1006/jcis.2000.6960

[8] Mustafa, S., Shahida, P., Naeem, A., Dilara, B. and Rehana, N. (2002) Sorption Studies of Divalent Metal Ions on ZnO. *Langmuir*, **18**, 2254-2259. https://doi.org/10.1021/la0014149

[9] Criscenti, L.J. and Sverjensky, D.A. (2002) A Single-Site Model for Divalent Transition and Heavy Metal Adsorption over a Range of Metal Concentrations. *Journal of Colloid and Interface Science*, **253**, 329-352. https://doi.org/10.1006/jcis.2002.8529

[10] Shakhapure, J., Vijayanand, H., Basavaraja, S. and Hiremath, V. (2005) Uses of α-Fe_2O_3 and Fly Ash as Solid Adsorbents. *Bulletin of Materials Science*, **28**, 713-718. https://doi.org/10.1007/BF02708542

[11] Lin, L.C., Thirumavalavan, M., Wang, Y.T. and Lee, J.F. (2010) Surface Area and Pore Size Tailoring of Mesoporous Silica Materials by Different Hydrothermal Treatments and Adsorption of Heavy Metal Ions. *Colloids and Surfaces A*: *Physicochemical and Engineering Aspects*, **369**, 223-231. https://doi.org/10.1016/j.colsurfa.2010.08.032

[12] Thirumavalavan, M., Wang, Y.T., Lin, L.C. and Lee, J.F. (2011) Monitoring of the Structure of Mesoporous Silica Materials Tailored Using Different Organic Templates and Their Effect on the Adsorption of Heavy Metal Ions. *The Journal of Physical Chemistry C*, **115**, 8165-8174. https://doi.org/10.1021/jp200029g

[13] Ma, Z., Ji, H., Teng, Y., Dong, G., Zhou, J., Tan, D. and Qiu, J. (2011) Engineering and Optimization of Nano- and Mesoporous Silica Fibers Using Sol-Gel and Electrospinning Techniques for Sorption of Heavy Metal Ions. *Journal of Colloid and Interface Science*, **358**, 547-553. https://doi.org/10.1016/j.jcis.2011.02.066

[14] Xia, K., Ferguson, R.Z., Losier, M., Tchoukanova, N., Bruening, R. and Djaoued, Y. (2010) Synthesis of Hybrid Silica Materials with Tunable Pore Structures and Morphology and Their Application for Heavy Metal Removal from Drinking Water. *Journal of Hazardous Materials*, **183**, 554-564. https://doi.org/10.1016/j.jhazmat.2010.07.060

[15] Stathi, P., Dimos, K., Karakassides, M.A. and Deligiannakis, Y. (2010) Mechanism of Heavy Metal Uptake by a Hybrid MCM-41 Material: Surface Complexation and EPR Spectroscopic Study. *Journal of Colloid and Interface Science*, **343**, 374-380. https://doi.org/10.1016/j.jcis.2009.11.029

[16] Ma, T.Y., Zhang, X.J. and Yuan, Z.Y. (2009) High Selectivity for Metal Ion Adsorption: From Mesoporous Phosphonated Titanias to Meso-/Macroporous Titanium Phosphonates. *Journal of Materials Science*, **44**, 6775-6785. https://doi.org/10.1007/s10853-009-3576-7

[17] Showkat, A.M., Zhang, Y.P., Kim, M.S., Gopalan, A.I., Reddy, K.R. and Lee, K.P. (2007) Analysis of Heavy Metal Toxic Ions by Adsorption onto Amino-Functionalized Ordered Mesoporous Silica. *Bulletin of the Korean Chemical Society*, **28**, 1985-1992.

https://doi.org/10.5012/bkcs.2007.28.11.1985

[18] Zhang, L., Yu, C., Zhao, W., Hua, Z., Chen, H., Li, L. and Shi, J. (2007) Preparation of Multi-Amine-Grafted Mesoporous Silicas and Their Application to Heavy Metal Ions Adsorption. *Journal of Non-Crystalline Solids*, **353**, 4055-4061. https://doi.org/10.1016/j.jnoncrysol.2007.06.018

[19] Sayari, A., Hamoudi, S. and Yang, Y. (2005) Applications of Pore-Expanded Mesoporous Silica. 1. Removal of Heavy Metal Cations and Organic Pollutants from Wastewater. *Chemistry of Materials*, **17**, 212-216. https://doi.org/10.1021/cm048393e

[20] Liu, A.M., Hidajat, K., Kawi, S. and Zhao, D.Y. (2000) A New Class of Hybrid Mesoporous Materials with Functionalized Organic Monolayers for Selective Adsorption of Heavy Metal Ions. *Chemical Communications*, **230**, 1145-1146. https://doi.org/10.1039/b002661l

[21] Brown, J., Richer, R. and Mercier, L. (2000) One-Step Synthesis of High Capacity Mesoporous Hg^{2+} Adsorbents by Non-Ionic Surfactant Assembly. *Microporous and Mesoporous Materials*, **37**, 41-48. https://doi.org/10.1016/S1387-1811(99)00191-2

[22] Mercier, L. and Pinnavaia, T.J. (1997) Access in Mesoporous Materials: Advantages of a Uniform Pore Structure in the Design of a Heavy Metal Ion Adsorbent for Environmental Remediation. *Advanced Materials*, **9**, 500-503. https://doi.org/10.1002/adma.19970090611

[23] Jhon, Q.T., Averlant, R., Giraudon, J.M. and Lamonjer, J.F. (2010) Mesoporous Manganese Oxide Catalysts for Formaldehyde Removal: Influence of the Cerium Incorporation. *Studies in Surface Science and Catalysis*, **175**, 517-520. https://doi.org/10.1016/S0167-2991(10)75098-9

[24] Hasegawa, Y., Fukumoto, K., Ishima, T., Yamamoto, H., Sano, M. and Miyake, T. (2009) Preparation of Copper-Containing Mesoporous Manganese Oxides and Their Catalytic Performance for CO Oxidation. *Applied Catalysis B: Environmental*, **89**, 420-424. https://doi.org/10.1016/j.apcatb.2008.12.023

[25] Sinha, A.K., Suzuki, K., Takahara, M., Azuma, H., Nonaka, T. and Suzuki, N. (2008) Preparation and Characterization of Mesostructured γ-Manganese Oxide and Its Application to VOCs Elimination. *The Journal of Physical Chemistry C*, **112**, 16028-16035. https://doi.org/10.1021/jp805211z

[26] Hong, X., Zhang, G., Zhu, Y. and Yang, H. (2003) Sol-Gel Synthesis and Characterization of Mesoporous Manganese Oxide. *Materials Research Bulletin*, **38**, 1695-1703. https://doi.org/10.1016/j.materresbull.2003.07.005

[27] Kragten, J. (1978) Atlas of Metal-Ligand Equilibria in Aqueous Solution. Ellis Horwood Limited, Chichester, 534.

[28] Cheng, J., Zou, X., Meng, X., Yang, G., Lu, X., Wei, C., Sun, Z., Feng, H. and Yang, Y. (2010) Lead Hydroxide Nanowires Obtained from Lead Nitrate Solution by Adding Chloride Ions. *Advanced Materials Research*, **123-125**, 719-722. https://doi.org/10.4028/www.scientific.net/AMR.123-125.719

[29] Bargar, J.R., Towle, S.N., Brown Jr., G.E. and Parks, G.A. (1996) Outer-Sphere Pb(II) Adsorbed at Specific Surface Sites on Single Crystal α-Alumina. *Geochimica et Cosmochimica Acta*, **60**, 3541-3547. https://doi.org/10.1016/0016-7037(96)00222-0

[30] Bargar, J.R., Towle, S.N., Brown Jr., G.E. and Parks, G.A. (1997) XAFS and Bond-Valence Determination of the Structures and Compositions of Surface Functional Groups and Pb(II) and Co(II) Sorption Products on Single-Crystal α-Alumina. *Journal of Colloid and Interface Science*, **185**, 473-492.

https://doi.org/10.1006/jcis.1996.4574

[31] Trivedi, P. and Axe, L. (2001) Predicting Divalent Metal Sorption to Hydrous Al, Fe, and Mn Oxides. *Environmental Science & Technology*, **35**, 1779-1784. https://doi.org/10.1021/es001644+

Electronic Supplementary Information (ESI)

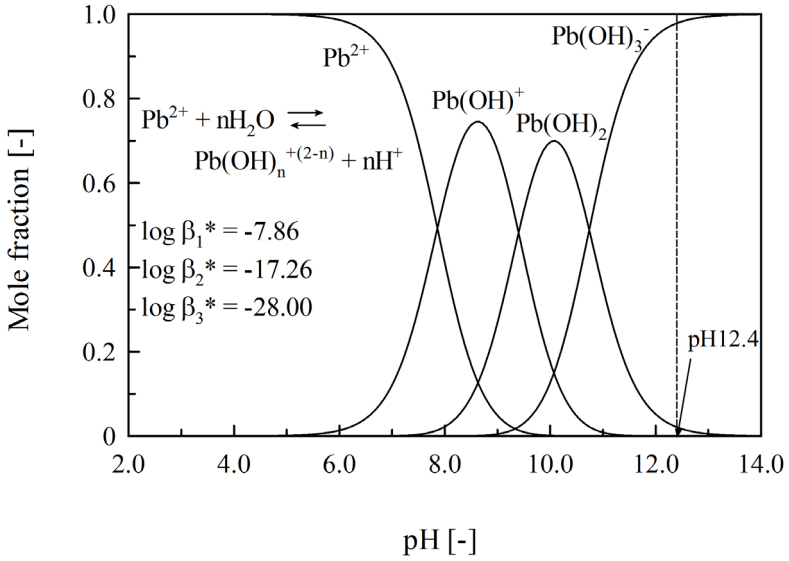

Figure S1. Calculated distribution diagram of Pb species in aqueous solution as a function of pH.

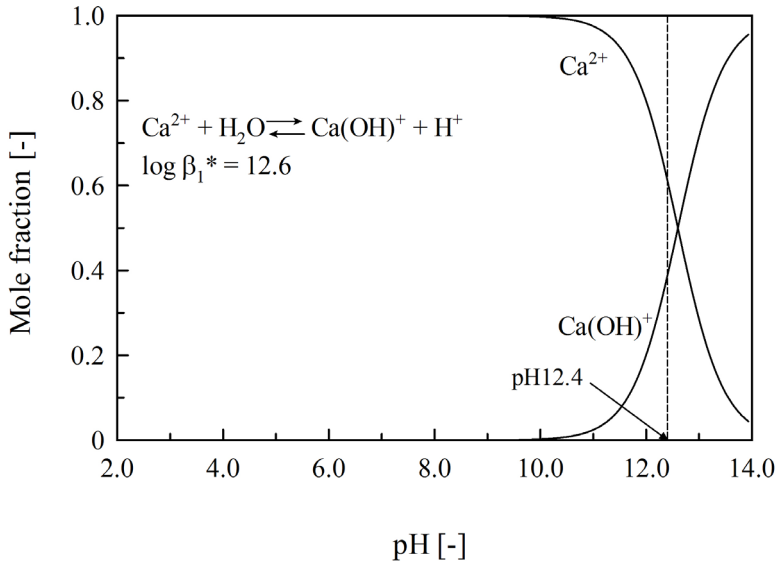

Figure S2. Calculated distribution diagram of Ca species in aqueous solution as a function of pH.